Immunomodulatory effect of a decellularized skeletal muscle scaffold in a discordant xenotransplantation model

Jonathan M. Fishman[a,b,c,d], Mark W. Lowdell[b], Luca Urbani[a], Tahera Ansari[c], Alan J. Burns[e], Mark Turmaine[f], Janet North[b], Paul Sibbons[c], Alexander M. Seifalian[g], Kathryn J. Wood[h], Martin A. Birchall[d], and Paolo De Coppi[a,i,1]

[a]Department of Surgery and [e]Neural Development Unit, University College London Institute of Child Health, London WC1N 1EH, United Kingdom; [b]Department of Haematology, Royal Free London National Health Service Trust and University College London, London NW3 2QG, United Kingdom; [c]Northwick Park Institute for Medical Research, Harrow, Middlesex HA1 3UJ, United Kingdom; [d]University College London Ear Institute and Royal National Throat, Nose, and Ear Hospital, University College London, London, WC1X 8DA, United Kingdom; [f]Division of Biosciences, University College London, London WC1N 1EH, United Kingdom; [g]Centre for Nanotechnology and Regenerative Medicine, University College London, London NW3 2PF, United Kingdom; [h]Transplantation Research Immunology Group, Nuffield Department of Surgical Sciences, University of Oxford, Oxford OX3 9DU, United Kingdom; and [i]Great Ormond Street Hospital for Children, London WC1N 3JH, United Kingdom

Edited by Yair Reisner, Weizmann Institute of Science, Rehovot, Israel, and accepted by the Editorial Board June 18, 2013 (received for review July 31, 2012)

Decellularized (acellular) scaffolds, composed of natural extracellular matrix, form the basis of an emerging generation of tissue-engineered organ and tissue replacements capable of transforming healthcare. Prime requirements for allogeneic, or xenogeneic, decellularized scaffolds are biocompatibility and absence of rejection. The humoral immune response to decellularized scaffolds has been well documented, but there is a lack of data on the cell-mediated immune response toward them in vitro and in vivo. Skeletal muscle scaffolds were decellularized, characterized in vitro, and xenotransplanted. The cellular immune response toward scaffolds was evaluated by immunohistochemistry and quantified stereologically. T-cell proliferation and cytokines, as assessed by flow cytometry using carboxy-fluorescein diacetate succinimidyl ester dye and cytometric bead array, formed an in vitro surrogate marker and correlate of the in vivo host immune response toward the scaffold. Decellularized scaffolds were free of major histocompatibility complex class I and II antigens and were found to exert anti-inflammatory and immunosuppressive effects, as evidenced by delayed biodegradation time in vivo; reduced sensitized T-cell proliferative activity in vitro; reduced IL-2, IFN-γ, and raised IL-10 levels in cell-culture supernatants; polarization of the macrophage response in vivo toward an M2 phenotype; and improved survival of donor-derived xenogeneic cells at 2 and 4 wk in vivo. Decellularized scaffolds polarize host responses away from a classical TH1-proinflammatory profile and appear to down-regulate T-cell xeno responses and TH1 effector function by inducing a state of peripheral T-cell hyporesponsiveness. These results have substantial implications for the future clinical application of tissue-engineered therapies.

Although replacement of airways (1–6) or urogenital tissue (7) using stem cell-based techniques has been achieved, engineering of functional contractile muscle tissue has only been partially explored (8–9). While debates have been generated around which myogenic progenitors (satellite cells, muscle stem cells, or myoblasts) should be used, fewer studies have focused on exploring which matrix could offer a better platform for regeneration (10, 11).

Autologous tissue-engineered solutions have the major advantage of not requiring immunosuppression, but clinical applications are limited to static organs and tissues, such as skin, or those that can function through passive movement alone, such as trachea, heart valves, blood vessels, and bladder (4, 7, 12). The field continues to expand and tissue bioengineering has provided, or is close to delivering, functional human organ replacements elsewhere (6, 7, 13–17). The ability to produce innervated and revascularized muscles would hugely extend the possible applications of regenerative medicine (18–26).

Decellularized skeletal muscle has been characterized by several groups, but its effect on cell-mediated immunity has not been studied (27–30). Here, we provide evidence that decellularized muscle scaffolds promote anti-inflammatory and immunosuppressive responses both in vitro and in vivo, down-regulate T-cell xeno responses and TH1 effector cytokines in vitro, and polarize the macrophage response in vivo toward an M2 phenotype (i.e., promote alternative pathway activation of macrophages).

Results

Decellularization Preserves the Extracellular Matrix and Down-Regulates MHC Classes I and II Expression. Efficient decellularization of rabbit cricoarytenoid dorsalis (CAD) muscles with preservation of extracellular matrix (ECM) structure was obtained by using a protocol consisting of latrunculin B, potassium chloride, potassium iodide, and DNase (27, 28). As shown, the use of a nondetergent, nonproteolytic protocol led to the preservation of the major components of the ECM (Fig. S1; ref. 27). Indeed, clearance of nuclei on H&E staining undetectable levels of DNA, with clearance of muscle-specific antigens (myosin heavy chain), were observed (Fig. S1 *A*, *D*, and *G*). Moreover, Miller's elastin staining showed a good preservation of elastin, which is concentrated around the vessels both in fresh and decellularized tissue (Fig. S1*F*). Picrosirius red staining showed the preservation of extracellular matrix collagen after decellularization process (Fig. S1 *B* and *E*) although its content ratio (collagen/wet tissue weight) decreased significantly in respect to the fresh tissue (Fig. S1*H*). Similarly, sulfated glycosaminoglycans quantification showed a progressive decrease in amount in the decellularized CAD (Fig. S1 *C* and *I*).

Both scanning and transmission electron microscopy of the decellularized muscle matrix showed the preservation of the micro and ultrastructural characteristics of the native tissue and confirmed the absence of cells. In particular, maintenance of a porous matrix, decellularization of existing blood vessels and nerves, eradication of nuclei and myofilaments, and preservation of collagen fibers were observed (Fig. S2).

Moreover, the biomechanical properties of decellularized tissue (DT) were preserved compared with fresh tissue (FT) (FT mean tensile Young's modulus = 38.89 ± 13.38; DT mean tensile Young's modulus = 48.30 ± 27.33; $P = 0.75$) (Fig. S3). Within fresh tissue, MHC class I expression was localized to the

Author contributions: J.M.F., M.W.L., K.J.W., and P.D.C. designed the study; J.M.F. and A.J.B. performed the experiments; T.A., M.T., J.N., P.S., and A.M.S. provided technical guidance; L.U. provided cell culture assistance; J.M.F. analyzed data, supported by M.W.L., L.U., and P.D.C.; and J.M.F., M.W.L., K.J.W., M.A.B., and P.D.C. wrote the paper.

The authors declare no conflict of interest.

This article is a PNAS Direct Submission. Y.R. is a guest editor invited by the Editorial Board.

[1]To whom correspondence should be addressed. E-mail: p.decoppi@ucl.ac.uk.

This article contains supporting information online at www.pnas.org/lookup/suppl/doi:10.1073/pnas.1213228110/-/DCSupplemental.

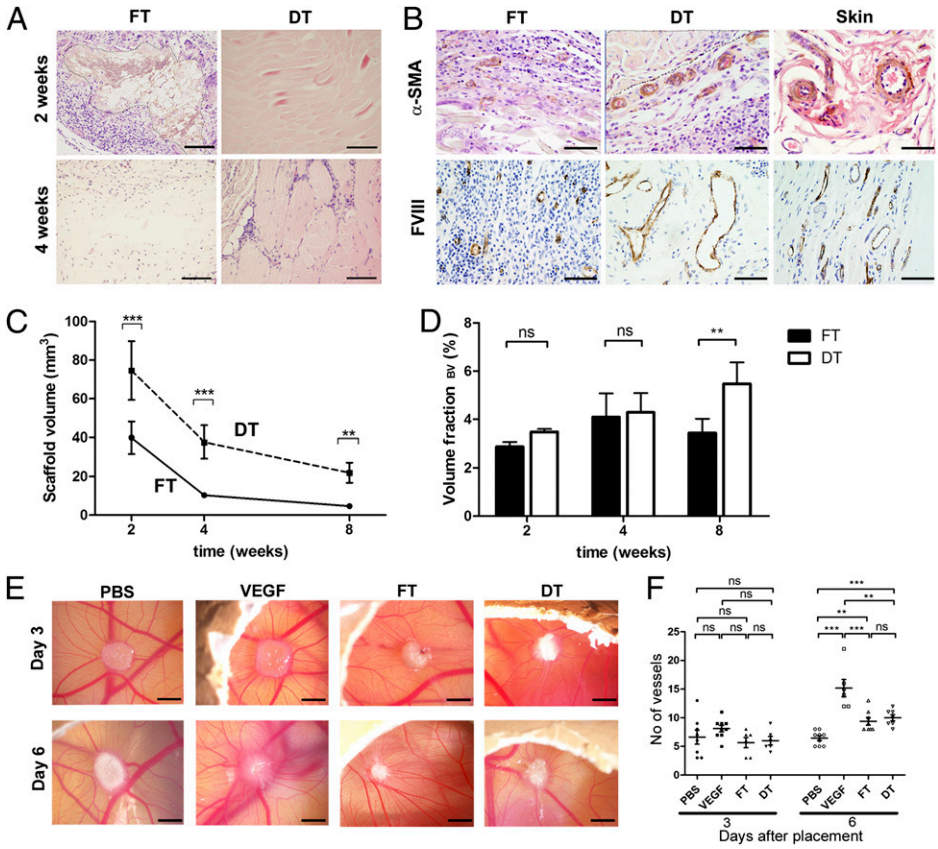

Fig. 1. Biocompatibility and proangiogenic properties of DT in vivo. (*A*) Biodegradation of FT and DT at 2 and 4 wk on H&E staining. Outline of FT at 2 wk is indicated in the figure by the dotted line. (B) α-smooth muscle actin staining at 2 wk and FVIII staining at 8 wk. α-smooth muscle actin positive blood vessels are seen at the interface of the host tissue and decellularized scaffold (as shown by dotted line) as early as 2 wk. Skin was used as a positive control in each case. (*C*) Quantification of FT and DT volume degradation by stereology (Cavalieri's method) over the course of the experiment (8 wk). (*D*) Volume fraction of blood vessels in FT and DT, respectively, representing the proportion of total tissue/scaffold volume occupied by blood vessels at 2, 4, and 8 wk, as quantified by stereology. (*E*) CAM assay. (*F*) CAM quantification of blood vessels ($n = 38$). Data in *F* presented as mean ± SEM. $n = 12$ scaffolds in each FT/DT group at each time-point. Statistical significance indicated by asterisks where ns, not significant; $^{**}P = 0.001$–0.01; $^{***}P < 0.001$. (Scale bars: *A*, 100 μm; *B*, 50 μm; *E*, 1 mm.)

endothelial cells of blood vessels (Fig. S4*A*). Decellularization was associated with a progressive decrease and absence of detectable levels of MHC class I and II antigens on endothelial cells and myofibers, respectively (Fig. S4 *B* and *E*).

Decellularization Slows Biodegradation Time in Vivo and Promotes an Efficient Angiogenic Response to the Transplanted Tissue. Decellularization significantly prolonged the time to complete biodegradation of the scaffold in vivo, whereas fresh tissue was rapidly degraded in a classical transplant rejection response (Fig. 1 *A* and *C*). In addition, new host blood vessels were seen at the interface between the host tissue and the decellularized scaffold as early as 2 wk after implantation as revealed by α-smooth muscle actin and factor VIII immunostaining (Fig. 1*B*). On the contrary, fresh tissue only triggered a minor angiogenic response, which may also have contributed to its fast degradation. As a consequence, DT was associated with a progressive increased volume fraction of blood vessels (Fig. 1*D*). Volume fractions were used as a measure of the functionality of the angiogenic response by the host toward the scaffold, representing the volume of implant occupied by blood vessels (31). The efficiency of the angiogenic response toward DT was confirmed by the chicken egg chorioallantoic membrane (CAM) assay (Fig. 1 *E* and *F*). The CAM findings support the conclusion that the degradation differences and vascularization effects seen in vivo are unlikely to be due to differences in the levels of proangiogenic growth factors between FT and DT. Given the comparability of the number of vessels in FT and DT implants within the CAM at day 6, we hypothesized that the degradation effects seen in vivo were due to the nature of the cellular infiltrates of the FT and DT implants, respectively.

Decellularized Scaffolds Polarize the Macrophage Response Toward an M2 Phenotype and Are Associated with a Significant Reduction in $CD3^+$ Cells in Vivo. We observed that implanted decellularized scaffolds in vivo were significantly associated with a decreased density of $CD3^+$ (9.65 ± 0.43 vs. 14.64 ± 1.88 cells $\times 10^{-5}$ μm^{-3}; $P = 0.0012$), $CD4^+$ (1.89 ± 0.04 vs. 4.98 ± 0.77 cells $\times 10^{-5}$ μm^{-3}; $P = 0.0159$) and $CCR7^+$ cells (7.46 ± 0.51 vs. 14.17 ± 3.38 cells $\times 10^{-5}$ μm^{-3}; $P = 0.0393$) in the surrounding tissues compared with implants of fresh tissue at 2 wk and an increase in the density of $CD163^+$ cells (7.35 ± 0.96 vs. 4.24 ± 0.75 cells $\times 10^{-5}$ μm^{-3}; $P = 0.0435$) (Figs. 2 and 3). Quantitative immunohistochemistry using CD86 and Arginase I (Arg I) as additional M1 and M2 markers supported these findings (6.82 ± 1.38 vs. 11.65 ± 0.81; $P = 0.0235$ for CD86 and 4.13 ± 0.47 vs. 1.75 ± 0.25; $P = 0.0041$ for Arg I). Additionally, we found a significant increase in $FoxP3^+$ cells at 2 wk (0.53 ± 0.03 vs. 0.28 ± 0.05; $P = 0.0159$) but not at other time points (Fig. 3).

Decellularized Scaffolds Decrease the T-Cell Proliferative Response in Vitro. In T-cell proliferation studies, when carboxyfluorescein diacetate succinimidyl ester (CFSE)-stained rat $CD3^+$ sensitized rat splenocytes were cocultured in the presence of either decellularized rabbit muscle scaffolds or fresh tissue acting as recall antigen, a significant reduction in T-cell proliferation was seen in

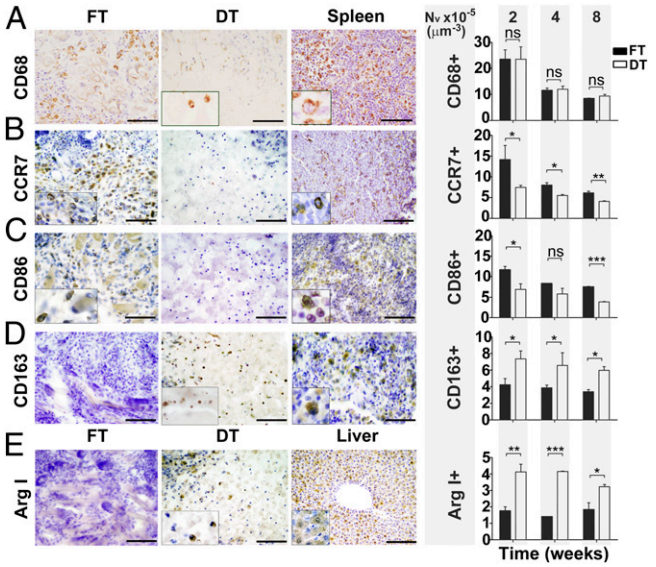

Fig. 2. Host macrophage response toward FT and DT in vivo at 2, 4, and 8 wk. (*A*) CD68 (pan-macrophage/monocyte marker). (*B*) CCR7 (M1 macrophage marker). (*C*) CD86 (M1 macrophage marker). (*D*) CD163 (M2 macrophage marker). (*E*) Arginase I (M2 macrophage marker). Two-week immunohistochemistry data are shown. (Scale bars: 50 μm.) *Insets* taken at higher power magnification. Spleen and liver were used as positive controls. The numerical density (N_V), as shown in the histograms, represents the number of cells across the scaffold per unit volume, as quantified by stereological techniques at 2, 4, and 8 wk. $n = 12$ scaffolds in each FT/DT group at each time-point. Statistical significance indicated by asterisks where ns, not significant; $*P = 0.01$–0.05; $**P = 0.001$–0.01; $***P < 0.001$.

the case of coculturing with decellularized scaffolds (proliferation index of 10.87 ± 2.56% vs. 2.10 ± 0.60%; $P = 0.0050$) (Fig. 4). The levels of T-cell proliferation seen were comparable to, and not significantly different from, those from the unstimulated condition (1.92 ± 0.46% vs. 2.10 ± 0.60%; $P = 0.85$). Stimulation with staphylococcal enterotoxin B (SEB) and/or unstained rabbit splenocytes (as part of a two-way mixed lymphocyte response (MLR), with stained rat splenocytes in a 1:1 ratio), resulted in the highest levels of T-cell proliferation seen after 72 h of cell culture, as expected (20.40 ± 1.70% for SEB and 22.20 ± 1.98% for MLR, respectively). Further phenotypic analysis revealed that the majority of the effects seen were due to a decrease in $CD4^+$ cells (Fig. S5).

Decellularized Scaffolds Modulate the Immune Response in Vitro Leading to Reduced Levels of Proinflammatory TH1 Cytokines and Increased Levels of Anti-Inflammatory and Suppressive TH2 Cytokines. Splenocytes collected from rats that received either fresh or decellularized tissues were cultured for 72 h and IL-2, IL-10, TNFα and IFN-γ concentrations were measured within the cell-free supernatants (Fig. 5). A significant decrease was seen in the supernatant concentrations of IL-2 (21.09 ± 3.15 vs. 51.41 ± 2.43 pg/mL; $P = 0.0065$) and IFN-γ (15.74 ± 8.16 vs. 114.8 ± 30.14 pg/mL; $P = 0.0281$) collected from rat splenocytes cocultured with decellularized scaffolds compared with the supernatants collected from splenocytes cocultured with fresh tissue. In contrast, a significant increase in IL-10 was observed (236.8 ± 26.05 vs. 15.47 ± 7.99 pg/mL; $P = 0.0013$). No significant difference was found in the concentrations of TNFα where, in both cases, the TNFα concentration measured was negligible (0.94 ± 0.94 vs. 9.52 ± 6.22 pg/mL; $P = 0.24$).

Decellularized Xenogeneic Scaffolds Improve the Survival of Xenogeneic Cells at 2 and 4 wk in Vivo. Given our previous data, we tested whether decellularized rabbit muscle scaffolds could support the survival of donor-derived mouse-EYFP myoblasts in a tibialis anterior injury model in immunocompetent rats (Fig. 6). SEM confirmed integration of cells into the scaffolds at the time of transplantation (Fig. 6 *A* and *B*). Improved donor cell survival at 2 and 4 wk was seen when donor cells were transplanted within decellularized scaffolds compared with poly(ε-caprolactone) scaffolds ($P < 0.001$) (Fig. 6 *D*, *E*, and *H*). There was no significant difference in survival between cell delivery via either a decellularized rabbit or rat scaffold, at both 2 wk (26.5 ± 9.95 vs. 20.8 ± 9.04 cells; $P = 0.65$) and 4 wk (21.1 ± 7.98 vs. 17.5 ± 9.44 cells; $P = 0.77$). Positivity of EYFP was confirmed by using an anti-EYFP antibody, and no staining was observed at either 2 or 4 wk in the contralateral (unoperated) limbs, sham controls, or animals that received scaffolds alone without cells. In addition, $CD163^+$ and $FoxP3^+$ cells were identified within the rabbit decellularized scaffolds at 2 and 4 wk (Fig. 6 *F* and *G*).

Discussion

This study demonstrates that decellularized scaffolds can modulate the immune response both by driving the macrophage response toward an M2 phenotype and by exhibiting anti-inflammatory and immunomodulatory effects in a xenotransplantation model. T-cell hyporesponsiveness as demonstrated by decreased T-cell proliferative response both in vitro and in vivo may be explained by the increased level of the inhibitory cytokine IL-10, and decreased levels of the proinflammatory cytokines IL-2 and IFN-γ, mediated by the presence of M2 monocytes either directly or through interaction with other T-cell subsets.

Decellularized skeletal muscle scaffolds that preserve the important constituents of the native ECM are biocompatible in vivo and exhibit noninflammatory effects (27). Moreover, decellularized muscle seeded with autologous myogenic cells can be used to functionally repair abdominal defects (22–23), and growth factors may further promote vascularization and, therefore, long-term functional results (21, 24). This study significantly adds to our previous data by demonstrating how the implanted scaffolds can modulate the immune response in several ways, thereby inhibiting rejection in a xenotransplantation model and preventing the rejection of donor-derived xenogeneic cells for up to 4 wk in vivo.

Interestingly, we observed polarization toward the M2 phenotype within the implanted scaffolds, as evidenced by the increase of $CD163^+$ and Arg I^+ cells and decrease of $CD86^+$ and $CCR7^+$ cells in decellularized implants. The parallel increase in $FoxP3^+$ T cells in the tissues surrounding the decellularized tissue implants suggests that these regulatory cells may have a role in the local modulation of the rejection response. The predominant phenotype of resident macrophages can provide an

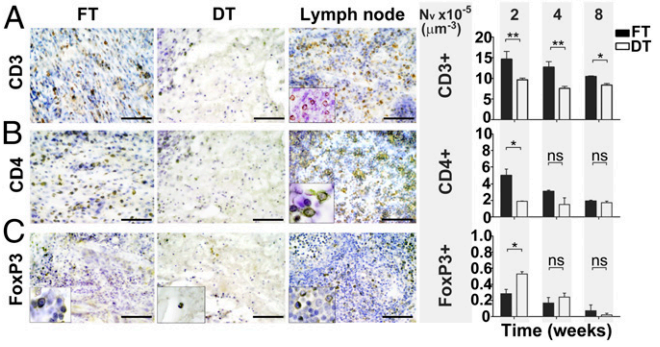

Fig.3. Host T lymphocyte response toward FT and DT in vivo at 2, 4, and 8 wk. (*A*) CD3 (T lymphocyte marker). (*B*) CD4 (Helper T-cell subset). (*C*) FoxP3 (Regulatory T-cell marker). Two-week immunohistochemistry data are shown. (Scale bars: 50 μm.) *Insets* taken at higher power magnification. Lymph node was used as a positive control. $n = 12$ scaffolds in each FT/DT group at each time-point. Statistical significance indicated by asterisks where ns, not significant; $*P = 0.01$–0.05; $**P = 0.001$–0.01.

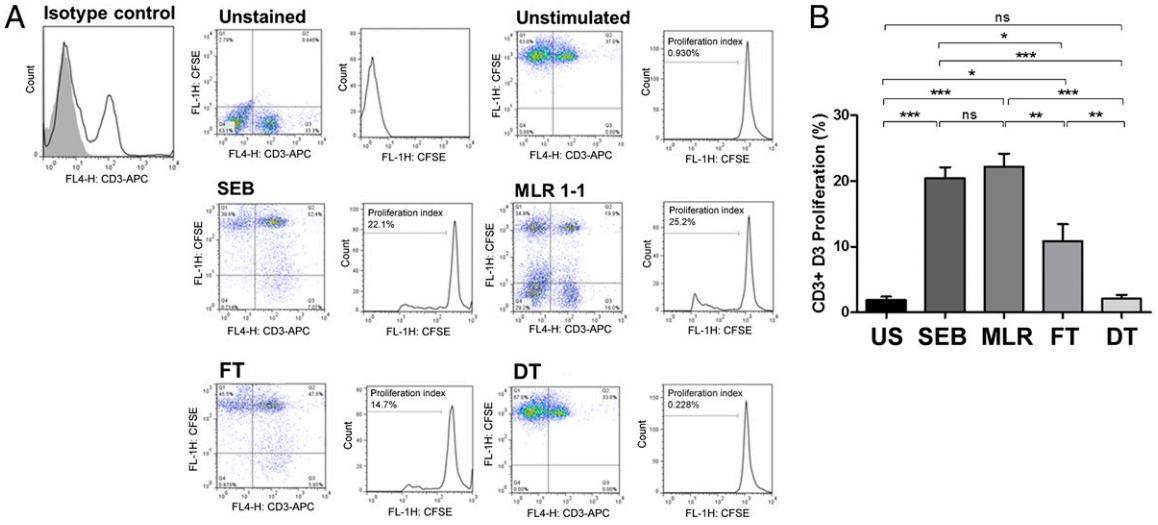

Fig. 4. Recall antigenic T-cell (CD3) proliferation assay by FACS analysis using CFSE dye. The percentage of proliferated $CD3^+$ cells were measured at day 3 (D3) culture and expressed as the proliferation index (i.e., the proportion of cells that have proliferated one, or more, times in response to the antigenic stimulus). (*A*) Representative samples of unstained cells (autofluorescence); unstimulated cells (negative control); SEB polyclonal mitogen (positive control); xenogeneic mixed lymphocyte response with a 1–1 stimulator (unstained rabbit splenocytes) to responder (stained rat splenocytes) ratio; coculture of CFSE-stained splenocytes with FT or DT, respectively. Isotype-matched negative control for comparison is shown in the figure. (*B*) Data across all samples at day 3 proliferation. US, unstimulated. $n = 8$ samples in each group. Statistical significance indicated by asterisks where ns, not significant; $*P = 0.01–0.05$; $**P = 0.001–0.01$; $***P < 0.001$.

indication of scaffold rejection (inflammation) or acceptance following implantation as shown (32, 33–40). M1-activated macrophages express IL-12^{high}, IL-23^{high}, and IL-10^{low} and produce inflammatory cytokines such as IL-1β, IL-6, and TNFα, which promote active inflammation, ECM destruction, and tissue injury. They are $CCR7^+$ $CD86^+$ and are inducer and effector cells in TH1-type inflammatory and rejection responses as observed when the fresh tissue was implanted. M2-activated macrophages, however, express an IL-12^{low}, IL-23^{low}, and IL-10^{high} phenotype and are able to facilitate tissue repair, constructive remodelling through ECM construction, and angiogenesis, which could partially be responsible for the regeneration observed when decellularized muscles are implanted (22, 23, 27). M2 macrophages are $CD163^+$ Arg I^+ and predominantly induce a classical TH2 response that is anti-inflammatory and is hypothesized to be particularly beneficial for constructive tissue remodelling and skeletal muscle regeneration (41, 42).

Our findings of a polarization toward an M2 phenotype are confirmed by the prolongation in biodegradation time of decellularized implants and the increase in donor angiogenesis of the decellularized tissue. Blood vessels were seen lining up at the interface of the host tissue and decellularized scaffold as early as 2 wk. Whether this phenomenon represents recellularization of existing decellularized blood vessels, or is secondary to true de novo angiogenesis, is uncertain. However, the speed of this process and the identification of decellularized blood vessels on transmission electron microscopy lend support to the former hypothesis.

Despite the major role played by the macrophages, other cellular and humoral immunological responses are likely to occur after decellularized scaffold implantation. Indeed, we demonstrate here that there is an attenuated TH1 cell-mediated immune response toward the decellularized scaffolds compared with fresh tissue. This effect could be driven both by the absence of the cells, which can trigger the immunoresponse, and by the fact that decellularization promotes anti-inflammatory and immunosuppressive effects both in vitro and in vivo. Evidence for the latter is shown here by a reduced T-cell proliferative response in vitro; increased production of the inhibitory cytokine IL-10 and decreased production of the proinflammatory cytokines, IL-2 and IFN-γ; a decreased T-cell response in vivo; and enhanced survival of xenogeneic cells within decellularized scaffolds for up to 4 wk in vivo.

Our findings are in agreement with previous studies that have demonstrated the highly confined immune responses toward decellularized scaffolds, and their anti-inflammatory effects (4, 27,

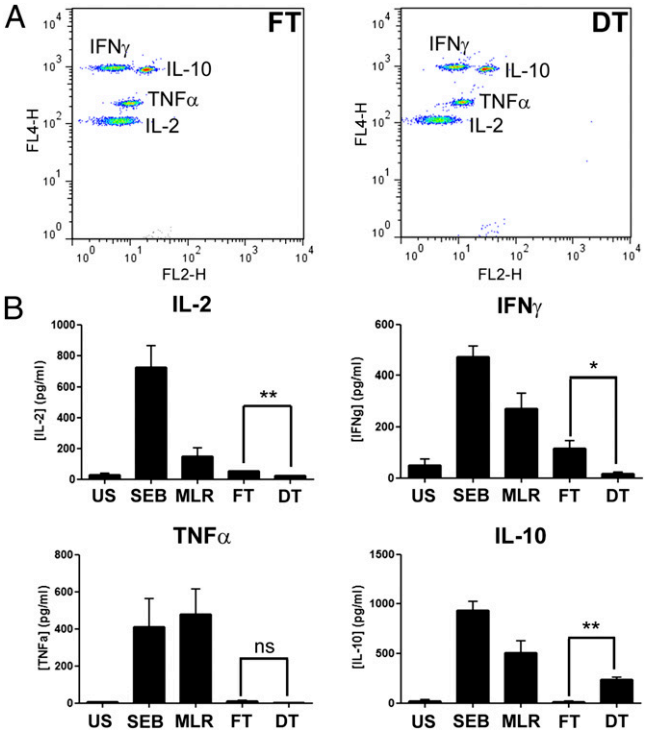

Fig. 5. Cytometric bead array measuring IL-2, IFN-γ, TNFα, and IL-10 cytokine concentrations within supernatants of cell suspensions. (*A*) Representative samples of supernatants collected from cocultures of stained rat splenocytes with FT or DT, respectively. (*B*) Data for IL-2, IFN-γ, TNFα, and IL-10 cytokine concentrations across all samples at day 3 proliferation. DT, decellularized tissue; FT, fresh tissue; MLR, mixed lymphocyte response; SEB, staphylococcal enterotoxin B; US, unstimulated. At least 3 samples were analyzed per group per cytokine. Statistical significance indicated by asterisks where ns, not significant; $*P = 0.01–0.05$; $**P = 0.001–0.01$.

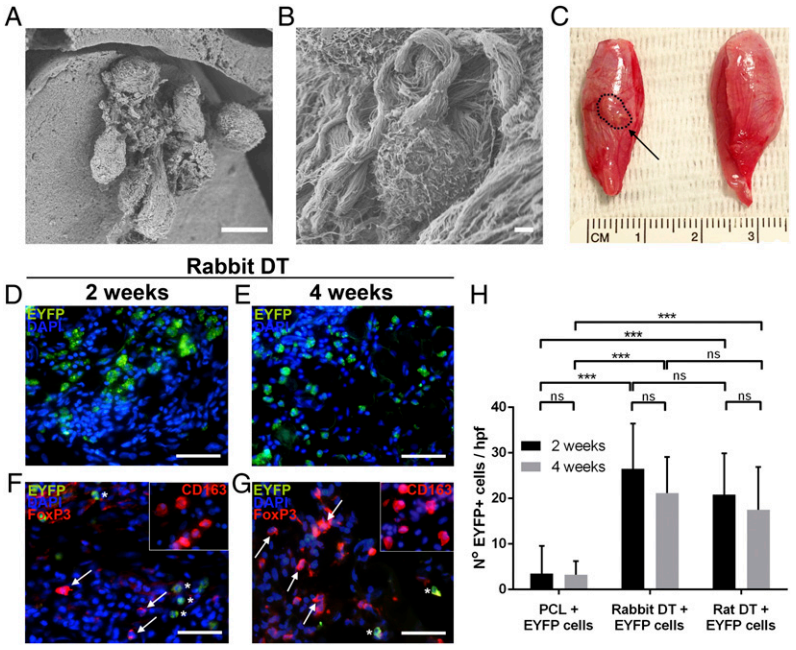

Fig. 6. DT seeded with donor-derived xenogeneic cells and transplanted into the tibialis anterior muscle of immunocompetent rats. (*A* and *B*) SEM images of seeded scaffolds at the time of transplantation. (*C*) Macroscopic appearance of scaffold (indicated by dashed line) after 2 wk in vivo demonstrating integration of the seeded scaffold into the surrounding tissue (*Left*) compared with contralateral (unoperated) side (*Right*). (*D* and *E*) $EYFP^+$ cells were identified within rabbit DT at 2 and 4 wk. (*F* and *G*) $FoxP3^+$ (shown by arrows) and $CD163^+$ cells (*Inset*) within rabbit DT at 2 and 4 wk. Donor-derived EYFP cells indicated by asterisks. (*H*) Overall number of $EYFP^+$ cells seen within each condition at 2 and 4 wk (hpf, high power field). $n = 38$ rats. Statistical significance indicated by asterisks where ns, not significant; $^{***}P < 0.001$. (Scale bars: *A*, 10 μm; *B*, 1 μm; *D*–*G*, 50 μm.)

43–47), which are probably beneficial to host integration of tissue-engineered material. The immunomodulatory effects seen may be partly ascribed to the removal or denaturing of MHC classes I and II molecules during decellularization. Donor-derived MHC class I, which immunolocalized preferentially to donor endothelial cells, became undetectable during decellularization, but was again measurable in the host blood vessels following implantation (host-derived MHC class I), in agreement with previous studies that have demonstrated evasion of rejection when the donor is vascularized by host blood vessels (48, 49). As well as a shift toward an M2-like phenotype with decellularization, we have also observed a shift away from a TH1 (as in classical acute rejection, for example) toward a TH2-like phenotype (generally associated with transplant acceptance), in agreement with previous studies (32, 50, 51).

How the decellularized scaffold modulates the host immune response remains to be determined. Low or zero levels of MHC classes I and II would explain the decreased T-cell proliferative response seen in vitro, the anti-inflammatory effects seen in vivo, and the reductions seen in IL-2 and IFN-γ through mitigation of direct T-cell antigenic presentation mechanisms. This explanation goes some way to accounting for our findings but fails to account for the increases seen in IL-10, as well as polarization of the macrophage response toward an M2 phenotype and the protection afforded by such scaffolds in preventing the rejection of xenogeneic donor cells. One hypothesis is that the process of decellularization exposes (unmasks) certain surface peptides and molecules on the scaffold that modulate the immune response (52, 53–55). Clearly, raised levels of IL-10 also raise the possibility of a response mediated by regulatory T cells which may be playing an integral role in the effects seen, as demonstrated in this study (56, 57). Finally, with regard to our in vitro results, we are unable to exclude nonspecific "bystander" effects, i.e., release of cytokines through stimulation of unrelated cells, or stimulation of unrelated T cells by cytokines during an antigen-specific T-cell response. Indeed, the spleen has been shown to act as a rich source of reservoir monocytes that are deployed to sites of inflammation (58). Further investigations are required to prove what cell subsets are true antigen-specific responders and what cells may be nonspecific bystanders. In addition, demonstration of prolonged allograft or xenograft survival in vivo would provide a compelling argument for the significance of the findings.

In conclusion, we demonstrate that decellularized skeletal muscle scaffolds can be generated that display highly desirable immunomodulatory activities in a discordant xenotransplantation model. Such scaffolds appear to skew the host response toward TH2 and M2 cell and cytokine profiles. These findings are of great importance in the design of new therapies based on tissue-engineering technology. Work is required to identify the precise mechanisms by which such scaffolds exert these effects.

Materials and Methods

Detailed materials and methods are listed in *SI Materials and Methods*. Preparation of decellularized scaffolds, quantitative immunohistochemistry, biocompatibility studies, T-cell proliferation assays, and transplantation experiments followed established procedures described in *SI Materials and Methods*. Histology, transmission and scanning electron microscopy, biomechanical studies, CAM assays, and cytometric bead arrays were conducted by using standard procedures detailed in *SI Materials and Methods*.

ACKNOWLEDGMENTS. We thank Dr. K. Newton for supplying SEB and Dr. Eaton for useful discussion. This work was supported by Medical Research Council (MRC) Grant MRC G1100397 and an MRC Centenary Award (to J.M.F.), Spark's Children's Charity, the Rooney Foundation, and The Royal College of Surgeons of England. Some laboratory work was supported by MRC Translational Stem Cell Research Committee Grant RegenVOX G1001539 (to M.A.B.), a Great Ormond Street Hospital Charity grant (P.D.C.) and by the Istituto di Ricerca Pediatrica Città della Speranza.

1. Fishman JM, et al. (2011) Airway tissue engineering. *Expert Opin Biol Ther* 11(12): 1623–1635.
2. Lange P, Fishman JM, Elliott MJ, De Coppi P, Birchall MA (2011) What can regenerative medicine offer for infants with laryngotracheal agenesis? *Otolaryngol Head Neck Surg* 145(4):544–550.
3. Baiguera S, et al. (2010) Tissue engineered human tracheas for in vivo implantation. *Biomaterials* 31(34):8931–8938.
4. Macchiarini P, et al. (2008) Clinical transplantation of a tissue-engineered airway. *Lancet* 372(9655):2023–2030.
5. Jungebluth P, et al. (2011) Tracheobronchial transplantation with a stem-cell-seeded bioartificial nanocomposite: A proof-of-concept study. *Lancet* 378(9808): 1997–2004.
6. Elliott MJ, et al. (2012) Stem-cell-based, tissue engineered tracheal replacement in a child: A 2-year follow-up study. *Lancet* 380(9846):994–1000.
7. Atala A, Bauer SB, Soker S, Yoo JJ, Retik AB (2006) Tissue-engineered autologous bladders for patients needing cystoplasty. *Lancet* 367(9518):1241–1246.
8. Baiguera S, et al. (2011) Development of bioengineered human larynx. *Biomaterials* 32(19):4433–4442.

9. Totonelli G, et al. (2012) Esophageal tissue engineering: A new approach for esophageal replacement. *World J Gastroenterol* 18(47):6900–6907.
10. Machingal MA, et al. (2011) A tissue-engineered muscle repair construct for functional restoration of an irrecoverable muscle injury in a murine model. *Tissue Eng Part A* 17(17-18):2291–2303.
11. Rossi CA, et al. (2011) In vivo tissue engineering of functional skeletal muscle by freshly isolated satellite cells embedded in a photopolymerizable hydrogel. *FASEB J* 25(7):2296–2304.
12. Dahl SL, et al. (2011) Readily available tissue-engineered vascular grafts. *Sci Transl Med* 3(68):ra9.
13. Song JJ, et al. (2013) Regeneration and experimental orthotopic transplantation of a bioengineered kidney. *Nat Med* 19(5):646–651.
14. Totonelli G, et al. (2012) A rat decellularized small bowel scaffold that preserves villus-crypt architecture for intestinal regeneration. *Biomaterials* 33(12):3401–3410.
15. Ott HC, et al. (2008) Perfusion-decellularized matrix: Using nature's platform to engineer a bioartificial heart. *Nat Med* 14(2):213–221.
16. Petersen TH, et al. (2010) Tissue-engineered lungs for in vivo implantation. *Science* 329(5991):538–541.
17. Uygun BE, et al. (2010) Organ reengineering through development of a transplantable recellularized liver graft using decellularized liver matrix. *Nat Med* 16(7): 814–820.
18. Koffler J, et al. (2011) Improved vascular organization enhances functional integration of engineered skeletal muscle grafts. *Proc Natl Acad Sci USA* 108(36): 14789–14794.
19. Levenberg S, et al. (2005) Engineering vascularized skeletal muscle tissue. *Nat Biotechnol* 23(7):879–884.
20. Borselli C, et al. (2010) Functional muscle regeneration with combined delivery of angiogenesis and myogenesis factors. *Proc Natl Acad Sci USA* 107(8):3287–3292.
21. Conconi MT, et al. (2009) In vitro and in vivo evaluation of acellular diaphragmatic matrices seeded with muscle precursors cells and coated with VEGF silica gels to repair muscle defect of the diaphragm. *J Biomed Mater Res A* 89(2):304–316.
22. De Coppi P, et al. (2006) Myoblast-acellular skeletal muscle matrix constructs guarantee a long-term repair of experimental full-thickness abdominal wall defects. *Tissue Eng* 12(7):1929–1936.
23. Conconi MT, et al. (2005) Homologous muscle acellular matrix seeded with autologous myoblasts as a tissue-engineering approach to abdominal wall-defect repair. *Biomaterials* 26(15):2567–2574.
24. De Coppi P, et al. (2005) Angiogenic gene-modified muscle cells for enhancement of tissue formation. *Tissue Eng* 11(7-8):1034–1044.
25. Boldrin L, et al. (2008) Efficient delivery of human single fiber-derived muscle precursor cells via biocompatible scaffold. *Cell Transplant* 17(5):577–584.
26. Boldrin L, et al. (2007) Satellite cells delivered by micro-patterned scaffolds: A new strategy for cell transplantation in muscle diseases. *Tissue Eng* 13(2):253–262.
27. Fishman JM, Ansari T, Sibbons P, De Coppi P, Birchall MA (2012) Decellularized rabbit cricoarytenoid dorsalis muscle for laryngeal regeneration. *Ann Otol Rhinol Laryngol* 121(2):129–138.
28. Gillies AR, Smith LR, Lieber RL, Varghese S (2011) Method for decellularizing skeletal muscle without detergents or proteolytic enzymes. *Tissue Eng Part C Methods* 17(4): 383–389.
29. Perniconi B, et al. (2011) The pro-myogenic environment provided by whole organ scale acellular scaffolds from skeletal muscle. *Biomaterials* 32(31):7870–7882.
30. Wolf MT, Daly KA, Reing JE, Badylak SF (2012) Biologic scaffold composed of skeletal muscle extracellular matrix. *Biomaterials* 33(10):2916–2925.
31. Gerhardt LC, et al. (2011) The pro-angiogenic properties of multi-functional bioactive glass composite scaffolds. *Biomaterials* 32(17):4096–4108.
32. Badylak SF, Gilbert TW (2008) Immune response to biologic scaffold materials. *Semin Immunol* 20(2):109–116.
33. Valentin JE, Stewart-Akers AM, Gilbert TW, Badylak SF (2009) Macrophage participation in the degradation and remodeling of extracellular matrix scaffolds. *Tissue Eng Part A* 15(7):1687–1694.
34. Brown BN, Valentin JE, Stewart-Akers AM, McCabe GP, Badylak SF (2009) Macrophage phenotype and remodeling outcomes in response to biologic scaffolds with and without a cellular component. *Biomaterials* 30(8):1482–1491.
35. Badylak SF, Valentin JE, Ravindra AK, McCabe GP, Stewart-Akers AM (2008) Macrophage phenotype as a determinant of biologic scaffold remodeling. *Tissue Eng Part A* 14(11):1835–1842.
36. Martinez FO, Sica A, Mantovani A, Locati M (2008) Macrophage activation and polarization. *Front Biosci* 13:453–461.
37. Keane TJ, Londono R, Turner NJ, Badylak SF (2012) Consequences of ineffective decellularization of biologic scaffolds on the host response. *Biomaterials* 33(6): 1771–1781.
38. Brown BN, et al. (2012) Macrophage phenotype as a predictor of constructive remodeling following the implantation of biologically derived surgical mesh materials. *Acta Biomater* 8(3):978–987.
39. Porta C, et al. (2009) Tolerance and M2 (alternative) macrophage polarization are related processes orchestrated by p50 nuclear factor kappaB. *Proc Natl Acad Sci USA* 106(35):14978–14983.
40. Ruffell D, et al. (2009) A CREB-C/EBPbeta cascade induces M2 macrophage-specific gene expression and promotes muscle injury repair. *Proc Natl Acad Sci USA* 106(41): 17475–17480.
41. St Pierre BA, Tidball JG (1994) Differential response of macrophage subpopulations to soleus muscle reloading after rat hindlimb suspension. *J Appl Physiol* 77(1):290–297.
42. Malerba A, et al. (2009) Selection of multipotent cells and enhanced muscle reconstruction by myogenic macrophage-secreted factors. *Exp Cell Res* 315(6):915–927.
43. Daly KA, et al. (2012) Damage associated molecular patterns within xenogeneic biologic scaffolds and their effects on host remodeling. *Biomaterials* 33(1):91–101.
44. Jungebluth P, et al. (2009) Structural and morphologic evaluation of a novel detergent-enzymatic tissue-engineered tracheal tubular matrix. *J Thorac Cardiovasc Surg* 138(3):586–593; discussion 592–593.
45. Go T, et al. (2010) Both epithelial cells and mesenchymal stem cell-derived chondrocytes contribute to the survival of tissue-engineered airway transplants in pigs. *J Thorac Cardiovasc Surg* 139(2):437–443.
46. Bayrak A, et al. (2010) Human immune responses to porcine xenogeneic matrices and their extracellular matrix constituents in vitro. *Biomaterials* 31(14):3793–3803.
47. Palmer EM, et al. (2002) Human helper T cell activation and differentiation is suppressed by porcine small intestinal submucosa. *Tissue Eng* 8(5):893–900.
48. Hecht G, et al. (2009) Embryonic pig pancreatic tissue for the treatment of diabetes in a nonhuman primate model. *Proc Natl Acad Sci USA* 106(21):8659–8664.
49. Dekel B, et al. (2003) Human and porcine early kidney precursors as a new source for transplantation. *Nat Med* 9(1):53–60.
50. Allman AJ, et al. (2001) Xenogeneic extracellular matrix grafts elicit a TH2-restricted immune response. *Transplantation* 71(11):1631–1640.
51. Allman AJ, McPherson TB, Merrill LC, Badylak SF, Metzger DW (2002) The Th2-restricted immune response to xenogeneic small intestinal submucosa does not influence systemic protective immunity to viral and bacterial pathogens. *Tissue Eng* 8(1):53–62.
52. Thomas AH, Edelman ER, Stultz CM (2007) Collagen fragments modulate innate immunity. *Exp Biol Med (Maywood)* 232(3):406–411.
53. Morwood SR, Nicholson LB (2006) Modulation of the immune response by extracellular matrix proteins. *Arch Immunol Ther Exp (Warsz)* 54(6):367–374.
54. Bollyky PL, et al. (2011) ECM components guide IL-10 producing regulatory T-cell (TR1) induction from effector memory T-cell precursors. *Proc Natl Acad Sci USA* 108(19): 7938–7943.
55. Bollyky PL, et al. (2009) Intact extracellular matrix and the maintenance of immune tolerance: High molecular weight hyaluronan promotes persistence of induced CD4+CD25+ regulatory T cells. *J Leukoc Biol* 86(3):567–572.
56. Sun L, Yi S, O'Connell PJ (2010) IL-10 is required for human CD4(+)CD25(+) regulatory T cell-mediated suppression of xenogeneic proliferation. *Immunol Cell Biol* 88(4): 477–485.
57. Wu J, et al. (2008) In vitro expanded human CD4+CD25+ regulatory T cells are potent suppressors of T-cell-mediated xenogeneic responses. *Transplantation* 85(12):1841–1848.
58. Swirski FK, et al. (2009) Identification of splenic reservoir monocytes and their deployment to inflammatory sites. *Science* 325(5940):612–616.